neuroimaging

MDPI

Article

Keep Making That Face and It Will Stay That Way: Cross-Cohort Prediction of Empathy from Task-Relevant Connectivity in Task-Free Data

Nicco Reggente [1], Roshni Lulla [2], Tiffany Durinski [1], Jonas Kaplan [2], Marco Iacoboni [3,4] and Leonardo Christov-Moore [1,2,4,*]

[1] Institute for Advanced Consciousness Studies, Santa Monica, CA 90403, USA; nicco@advancedconsciousness.org (N.R.)
[2] Brain and Creativity Institute, University of Southern California, Los Angeles, CA 90007, USA; lulla@usc.edu (R.L.); jtkaplan@usc.edu (J.K.)
[3] Ahmanson-Lovelace Brain Mapping Center, Department of Psychiatry and Biobehavioral Sciences, University of California, Los Angeles, CA 90095, USA; iacoboni@ucla.edu
[4] Consciousness Center of Oaxaca, Oaxaca 68001, Mexico
* Correspondence: leo@advancedconsciousness.org

Abstract

Background/Objectives: Deficits in empathic function have deleterious effects on individual, relational, and community well-being, impacting long-term health outcomes. However, assessing empathic function in neurodivergent or nonverbal populations using self-reports and in-scanner tasks is frequently unfeasible. Encouraging evidence suggests that characteristic interactions in brain networks underlying empathy are observable at rest, though single-cohort approaches have been shown to limit replicability and generalizability. Methods: We tested whether machine learning-aided (LASSO) models trained and tested on connectivity matrices derived from task-free fMRI data in two cohorts of healthy participants (N = 96) could predict subdimensions of empathy when trained on one cohort and tested on the other. Results: We found that all subdimensions could be robustly predicted from our theory-driven networks, while classical resting-state networks only significantly predicted empathic concern and personal distress. Theory-driven networks matched or outperformed whole-brain models despite containing orders of magnitude fewer features, suggesting that a priori task-derived networks constrain resting-state analyses by concentrating predictive signal rather than relying on regularization to filter large feature spaces. Conclusions: Empathic function emerges from characteristic interactions within and between affective "resonance" and cognitive "control" networks. Empathic concern emerges as the most widely subserved and predictable sub-dimension, suggesting utility for diagnosis and intervention. Cross-cohort approaches hold potential for robustly assessing empathic function in heterogeneous cohorts, even those unable to complete traditional empathy tasks. We provide the model and dataset, to facilitate research and clinical applications by other groups and in vulnerable populations.

Keywords: empathy; fMRI; resting state; machine learning; cognitive neuroscience; functional connectivity; cross-cohort validation

Academic Editor: Daniele Corbo

Received: 26 November 2025
Revised: 21 April 2026
Accepted: 15 May 2026
Published: 2 July 2026

Key Contribution: This study establishes that trait empathy and its sub-dimensions can be robustly classified across independent cohorts—training on one and testing on the other—using a priori, task-defined resonance and control networks, demonstrating that these functional networks retain enough construct-relevant information at rest to match or exceed whole-brain models while using orders of magnitude fewer features.

1. Introduction

Empathy allows human and nonhuman animals to infer and share in the internal states of others [1–4]. It promotes harm aversion, empathic concern and prosocial behavior towards others, and facilitates cultural learning and coordinated behavior [5–7]. Empathy is a foundational aspect of social cognition, deficits in which are a core phenotype of numerous clinical conditions, as shown by a meta-analysis of 30 clinical conditions [8]. Social cognitive deficits predict symptoms of mental illness [9], disability severity and increased use of mental health resources, including hospital admissions and emergency visits [10]. The subjective and functional qualities of empathy may rely on our reflexive ability to process others' pain, visceral sensations and emotions much as we do our own, while maintaining active control over this vicarious processing [2,4,11].

This tendency to simulate others' internal states can be called self–other resonance (resonance for short, [2]). Research suggests that its likely substrate is neural resonance, the frequently observed overlapping activation for self-experienced or other-observed somatosensation, interoception, affect, and motor behavior [4,12,13]. We treat the sensorimotor, affective, visceral, and interoceptive areas implicated in this process as key nodes in a putative 'resonance' network within this manuscript. This controlled resonance with others extends beyond perception into behavior. Humans and other social animals mimic each other's behavior, reflexively and often without awareness, and below the threshold for observable behavior [2,14–17]. Behavioral mimicry occurs involuntarily when certain areas of the prefrontal cortex are damaged, suggesting it is both reflexive and controlled [18]. The vicarious somatomotor, interoceptive and affective processing emerging from resonance also informs our conscious evaluations of others' internal states, beliefs, and intentions [2,19–22]. Inhibition of somatosensory areas using transcranial magnetic stimulation impacts emotional empathy scores, supporting a social function for motor and neural resonance [23]. Resonance likely also influences our feelings and decisions about others' welfare [2,24–30], promoting empathic concern [31–34] and many forms of prosocial inclination, such as nonstrategic altruism in the Dictator Game [2], harm aversion in moral dilemmas [24], donations to reduce pain to another [35], everyday helping behavior [36,37], charitable donations [38], and even vicarious reward [39].

Resonance processes are modulated by top–down control systems involved in cognitive–sensory integration, decision-making and executive control, which integrate contextual information and conscious appraisal toward behavior and decision making [40–52]. Association cortices—including the temporoparietal junction (TPJ), dorsomedial and dorsolateral prefrontal cortex (DMPFC and DLPFC)—may then subsequently implement these modulatory effects, acting as key nodes in what we call the "control" network in this and past work. Indeed, disruptive neuromodulation of DMPFC and DLPFC causes a decrease in the inhibitory influence of context on prosocial behavior [30]. Transcranial magnetic stimulation (TMS) on the right supramarginal gyrus (rSMG), a sub-region of the TPJ, interferes with self–other distinction and empathic concern [53]. Lesions in the prefrontal cortex positively correlate with compulsive mimicry, indicating that resonance-controlling mechanisms remain active until damaged [18]. Numerous studies attest to complex, dynamic,

yet characteristic interaction between resonance and control systems during passive observation of emotions or pain [2], passive observation of films depicting personal loss [54], reciprocal imitation [17], tests of empathic accuracy [55], and comprehension of others' emotions [56].

This emphasis on information flow, and dynamic view of bottom–up perception vs. top–down regulation [57] is mirrored in our resonance/control framework, and choice of regions-of-interest (STS/IFG for perception, DLPFC/MPFC/Precuneus for regulation) associated with resonance and control (which we will refer to throughout as "resonance network" and "control network"), respectively. It also informs our choice to employ the resonance/control terminology vs. other comparable dual process taxonomies rooted in psychological or functional distinctions, i.e., cognitive/affective, vicarious experience/intuitive understanding [58], action understanding/mental inference [59], or mirroring/mentalizing [60], as "control" systems are also associated with the cognitive aspect of empathy, a.k.a. mentalizing [60], or intuitive understanding [58].

There has been an increased use of resting-state data in predicting behavioral traits, based on the assumption that long-term patterns of network interactions during active behavior and cognition may be reflected in characteristic patterns of interaction at rest. Using resting-state functional connectivity (rsFC), researchers have been able to predict narcissism [61], changes in trust and reciprocity [62], sex-specific differences in personality scores on the "Big 5" (neuroticism, openness, conscientiousness, agreeableness, extraversion) [63] measure [64]. Several studies have taken this approach to predicting empathic dispositions. Spies et al. [65] utilized an ultra-high-field 7T fMRI to characterize resting-state functional connectivity changes following gender transition, linking network-level connectivity shifts to measures of empathic responding. Abram et al. [66] applied seed-based functional connectivity to fronto-temporal circuits, demonstrating that reduced connectivity within this network predicted both cognitive empathy deficits and experiential negative symptoms in individuals with schizophrenia. Esmenio et al. [67] investigated effective connectivity across the default mode network and measured the influence of behavioral empathy subscales on connectivity parameters using a canonical variate analysis. Stoica and Depue [68] associated independent components (derived from ICA) with the Interpersonal Reactivity Index (IRI) [5] and Multidimensional Assessment of Interoceptive Awareness (MAIA) [69], finding that increased resting-state BOLD in mentalizing networks correlated with perspective-taking and mind–body interconnectedness. Winters et al. [70–72] identified network-level associations with behavioral measures of cognitive versus affective empathy and ranking predictive seed regions. Bray et al. [73] examined resting-state functional connectivity in children and its relationship to affective empathy, identifying connectivity patterns within and between networks associated with socio-affective processing. Ebisch et al. [58] applied graph theoretical measures of resting-state networks to predict two proposed dimensions of empathy—vicarious experience and intuitive understanding.

Underlying these approaches is the belief that patterns of neural connectivity reflective of "active" behavior, cognitive and affective processes can be observed even when the participant is not actively participating in those processes. This has an added benefit of permitting researchers to assess individual differences without the need for subjects to comprehend task or questionnaire instructions, which may be essential in populations that are unable to fulfill traditional neuropsychological tasks due to motor or cognitive deficits, differences in performance or even effort, making it difficult to interpret brain activation differences between populations. Hence, the potential clinical utility of task-free methods is promising.

We have characterized interactions between resonance and control network nodes' contributions to prosocial behavior using generalized psychophysiological interaction [74],

showing that connectivity between hubs of resonance and control networks was itself anticorrelated with prosocial behavior [2], and that disruptions to control nodes caused predicted increases in prosocial behavior [30]. More recently, we leveraged a machine learning-augmented form of multiple regression analysis used to predict treatment outcomes in OCD of resting-state data [75] to investigate individual differences in empathic function arising from resting connectivity patterns between resonance and control processes [76]. We used a least absolute shrinkage and selection operator (LASSO) regression model, a form of multiple regression constrained by regularization with built-in dimensionality reduction (i.e., shrinkage), on participants' functional connectivity pairwise correlation matrices [75]. Within a cross-validation framework, LASSO permitted us to make highly accurate predictions of unseen individuals' empathy behavioral scores while avoiding overfitting. We found that resting-state fMRI connectivity patterns within and between resonance and control networks predicted trait empathic concern in a single cohort of adults more robustly than canonical intrinsic networks [76]. The current study is a more robust extension of this approach.

Our goal here was to derive a more complete, multivariate understanding of how subfacets of trait empathy are represented and predicted by connectivity within and across these networks, using a robust method of training on one cohort, testing on the other, and averaging predictive values between the two approaches to reinforce generalizability, in line with contemporary proposals to use more heterogeneous, multi-cohort approaches in predictive neuroscience [77].

We propose that interactions between resonance and control networks measured by functional connectivity may be the basis for understanding individual differences in empathic dispositions, and that these interactions are stable enough across task demands to be observable at rest, allowing us to fruitfully interrogate resting-state data using task-related networks. This, combined with cross-cohort approaches, may prove a robust, targeted use of resting-state data in a time when there is an increasing sense that we have 'squeezed the lemon enough' with resting-state scans [78].

Here we sought to ascertain the robustness of our past work [76] leveraging a novel cohort (n = 47), and include the fantasizing subscale of the IRI [5], which was neglected in our last manuscript. Using this more exacting and generalizable method we sought to test the hypothesis that theory-derived resonance and control network interconnectivity at rest predicts the empathic concern trait as well or better than classical intrinsic brain networks. Since we only made an a priori prediction regarding pairs of networks concerned, Resonance + Control, we did not examine the predictive power of other pairs of networks, given the large amount of possible permutations (and hence tests to be accounted for in multiple comparison corrections) of networks, and our paucity of hypotheses regarding them. However, to control for the possibility that simply having more nodes would increase predictive power, we included the "all nodes" network in all analyses.

2. Materials and Methods

2.1. Participants

The current cohort comprises 47 equivalently recruited participants aged 18–26 (23 female) scanned at the Ahmanson-Lovelace Brain Mapping Center at UCLA on a Siemens Trio 3T, Siemens Healthineers, Erlangen, Germany between January 2015 and June 2016. Participants in the original cohort were 51 ethnically diverse, typically developing adults aged 18–35 (26 female) scanned at the same location and scanner between May 2013 and November 2014 (reported in [76]). All recruitment and experimental procedures were performed under approval of UCLA's institutional review board, in accordance with the ethical standards of the institutional and/or national research committee and with

the 1964 Helsinki declaration and its later amendments or comparable ethical standards. Informed consent was obtained from all individual participants included in the study.

Eligibility criteria for participants was assessed during preliminary screening interviews conducted by phone and included: right-handed, no prior or concurrent diagnosis of any neurological, psychiatric, or developmental disorders, and no history of drug or alcohol abuse.

2.2. Trait Empathy Assessment

Participants filled out the Interpersonal Reactivity Index (IRI) either at the end or beginning of each experimental session in a closed room, unobserved. The IRI [5] is a widely used [31,33] and validated [79] questionnaire designed to measure both cognitive and emotional components of empathy. It consists of 24 statements that the participant rates on a 5-point scale ranging from 0 (does not describe me well) to 5 (describes me very well). The statements are calculated to test four theorized subdimensions of empathy:

- Fantasizing Scale (FS): Appears to tap the tendency to imaginatively transpose oneself into fictional situations (e.g., books, movies, daydreams).
- Perspective-Taking (PT): seems to reflect an ability or proclivity to shift perspectives—to step "outside the self"—when dealing with other people.
  The other two subscales explicitly deal with individual differences in emotional responses to observed emotionality in others.
- Empathic Concern (EC): Assesses the degree to which the respondent experiences feelings of warmth, compassion, and concern for the observed individual.
- Personal Distress (PD): Measures the individual's own feelings of fear, apprehension and discomfort at witnessing the negative experiences of others.

2.3. Functional MRI Data Collection

All neuroimaging data was acquired via a series of MRI scans conducted in a Siemens Trio 3T scanner housed in the Ahmanson-Lovelace Brain Mapping Center at UCLA. Resting data were collected while participants passively observed a white fixation cross on a black screen. They were instructed only to "Look at the fixation cross and just let your mind wander." Resting-state functional images for both cohorts were acquired over 36 axial slices covering the whole cerebral volume using an echo planar T2*-weighted gradient echo sequence (6 min; TR = 2500 ms; TE = 25 ms; flip angle = 90 degrees; matrix size = 64 × 64; FOV 20 cm; in-plane resolution = 3 mm × 3 mm; slice thickness = 3 mm/1 mm gap). A T1-weighted volume was also acquired in each participant (TR = 2300 ms, TE = 25 ms, TI = 100 ms, flip angle = 8°, matrix size = 192 × 192, FOV = 256 cm, 160 slices, voxel size 1.3 × 1.3 × 1.0 mm).

2.4. Functional MRI Preprocessing

Functional MRI preprocessing was performed in FEAT (FMRI Expert Analysis Tool, Version 6.0.4), part of FSL (FMRIB's Software Library). After motion correction using MCFLIRT, images were temporally high-pass filtered with a cutoff period of 100 s (equivalent to 0.01 Hz) and smoothed using a 6 mm Gaussian FWHM algorithm in 3 dimensions. Our protocol stipulated that participants showing absolute or relative head motion exceeding 1 mm were excluded from further analyses, though no participants exceeded this threshold.

In order to remove non-neuronal sources of coherent oscillation in the relevant frequency band (0.01–0.1 Hz), preprocessed data was subjected to probabilistic independent component analysis as implemented in MELODIC (Multivariate Exploratory Linear Decomposition into Independent Components) Version 3.10, part of FSL. Noise components

corresponding to head motion, scanner noise, cardiac/respiratory signals were identified by observing their localization, time series and spectral properties and removed using FSL's regfilt command [80].

Each participant's functional data was coregistered to standard space (MNI 152 template) via registration of an averaged functional image to the high resolution T1-weighted volume using a six degree-of-freedom linear registration and of the high-resolution T1-weighted volume to the MNI 152 template via nonlinear registration, implemented in FNIRT.

2.5. Designation of Regions of Interest

All networks were created by pooling from a set of 198 5 mm spherical ROIs. A total of 196 of the ROIs were derived from a functionally derived cortical atlas [81]. We also included an additional pair of 5 mm ROIs centered on the left (x = −22 mm, y = −6 mm, z = −14 mm) and right (x = 22 mm, y = −6 mm, z = −14 mm) amygdala, as this region was not included in the original cortical atlas. We used ROIs from the following networks defined by [81] Visual (31 ROIs), Fronto-parietal (25 ROIs), Somatosensory–Motor (25 ROIs), Dorsal Attention (11 ROIs), Ventral Attention (9 ROIs), Salience (18 ROIs), Memory Retrieval (5 ROIs), Cingulo-opercular (14 ROIs), and default mode (58 ROIs) networks.

In the prior study, two theory-driven networks (bottom–up resonance and top–down control) were created by selecting ROIs from the Power cortical atlas overlapping with brain areas associated with neural resonance and top–down control [76]. Resonance areas included the core cortical imitation circuitry (inferior frontal gyrus, inferior parietal lobule, superior temporal sulcus; [82]), as well as insular, limbic (bilateral amygdala) and somatomotor areas associated with neural resonance for visceral sensation, emotion, pain and motor behavior [4,59]. This putative bottom–up resonance network (Power–Resonance) consisted of 34 ROIs. Control areas included dorsolateral prefrontal cortex, temporoparietal junction, lateral orbitofrontal cortex and sites covering a range from dorsal to ventral medial prefrontal and paracingulate cortex, implicated in the top–down regulation of spontaneous and deliberate imitation, affect and pain [2,76,83–91]. This putative top–down control network (Power–Control) consisted of 22 ROIs. This allowed us to test our conceptual model of resonance–control network interaction as a substrate for empathic concern [2,76], while constraining ROI locations to those defined in [81] and assigning these ROI locations to the two networks on the basis of the existing literature. See Table S1 for a list of ROIs used to define the resonance and control networks and Figure 1 for a visual rendering of the same ROIs/networks.

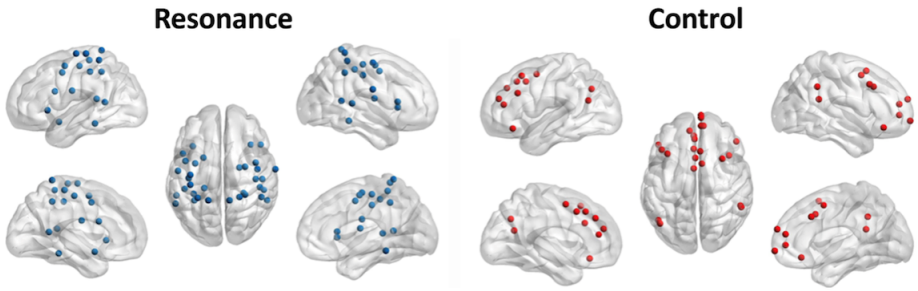

Figure 1. Functional ROI atlases' instantiations of the theory-driven resonance (**left**; blue) and control (**right**; red) networks derived from a combination of the [81] cortical atlas and bilateral amygdala ROIs.

2.6. Machine Learning Analyses

2.6.1. Feature Creation

For each participant, mean BOLD time courses were extracted from the average activity across voxels within each ROI. Matrices of pairwise Pearson correlation coefficients were created by correlating each ROI's BOLD time course with every other ROI within

each network, generating a set of features (non-redundant functional connectivity values) for each participant, network, and behavioral measure of interest (i.e., the IRI subscales). For "between-networks" analyses, ROIs belonging to each pair of networks being studied (e.g., Power–Resonance and Power–Control) were concatenated and treated as a single network, allowing for pairwise connectivity across both networks' ROIs. To account for potential covariation due to robust sex differences in empathic function [88], participant sex was iteratively regressed out of each feature, and the residuals were subsequently used as the functional connectivity features.

2.6.2. Parameter Optimization

For each behavioral measure, the LASSO regularization parameter (λ) was optimized independently within each cohort using leave-one-out cross-validation. In each fold, a LASSO model was fit across 100,000 candidate lambda values (0.0001 to 10, in increments of 0.0001), and predictions were generated for the held-out subject at each lambda. The lambda yielding the highest Pearson correlation between predicted ($\hat{y}$) and actual (y) values across all folds was selected as optimal for that cohort. The two cohort-specific lambdas were then averaged to obtain a single lambda for cross-cohort prediction.

2.6.3. Cross-Cohort Classification

Using the averaged λ, two LASSO models were trained—one on each cohort—and tested on the other. Prediction accuracy was quantified using Pearson's correlation coefficient between predicted ($\hat{y}$) and observed (y) values:

$$r = \frac{\sum(\hat{y}_i - \bar{\hat{y}})(y_i - \bar{y})}{\sqrt{\sum(\hat{y}_i - \bar{\hat{y}})^2 \cdot \sum(y_i - \bar{y})^2}} \quad (1)$$

Prediction error was quantified using root mean squared error:

$$\text{RMSE} = \sqrt{\frac{1}{n}\sum(\hat{y}_i - y_i)^2} \quad (2)$$

Accuracy is defined throughout as Pearson's r between predicted and observed values; variance explained (R^2) is additionally reported as the square of r. Both metrics were computed for each direction (train Cohort 1 $\rightarrow$ test Cohort 2, and vice versa). Overall accuracy and RMSE were calculated as the mean across both directions. To estimate uncertainty, 95% confidence intervals for r were derived via bootstrap resampling (10,000 iterations with replacement) of predicted–observed pairs. Figure 2 showcases the full machine learning analysis workflow.

To assess model complexity, the number of non-zero LASSO coefficients was recorded for each cross-cohort direction. Feature selection stability was quantified as the overlap between the two directions—specifically, the number of edges assigned non-zero coefficients in both the train Cohort 1/test Cohort 2 and train Cohort 2/test Cohort 1 models, expressed as a percentage of the union of selected edges across both directions.

2.6.4. Significance Testing

Statistical significance was assessed via permutation testing (10,000 iterations). In each iteration, training labels within each cohort were independently shuffled, and the full cross-cohort prediction procedure (Section 2.6.3) was repeated using the same averaged lambda. P-values were calculated as the proportion of permutation-derived accuracies greater than or equal to the observed accuracy.

2.6.5. Correction for Multiple Comparisons

Each IRI subscale was treated as a separate family for multiple comparisons correction. False discovery rate (FDR) correction was applied to all permutation-derived p-values across networks and network combinations within each subscale using the Benjamini–Hochberg procedure [92]. Corrected p-values were considered significant at $p < 0.05$ (one-tailed).

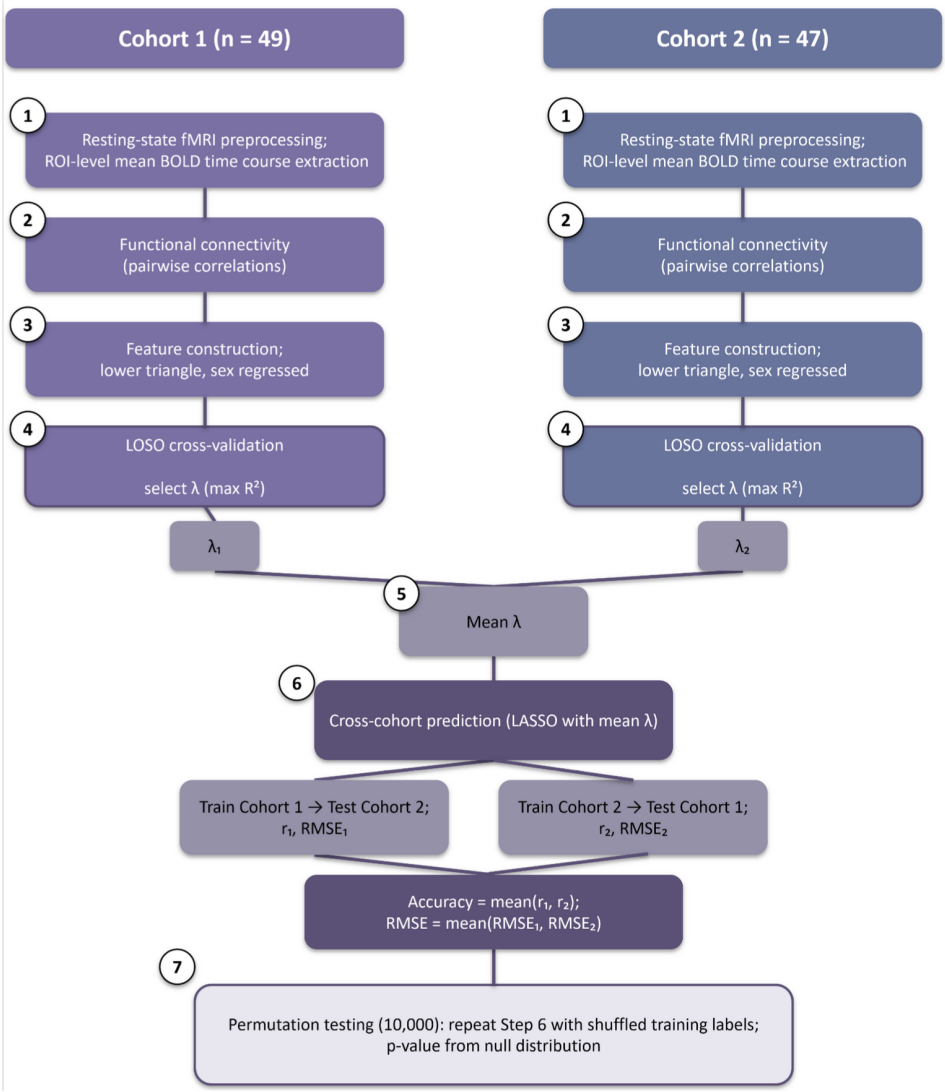

Figure 2. Cross-cohort LASSO prediction pipeline for a single IRI subscale and network. Steps 1–4 proceed independently for each cohort: resting-state fMRI is preprocessed and mean BOLD time courses are extracted from regions of interest (ROIs) within the network of interest (Step 1), pairwise Pearson correlations are computed (Step 2), the lower triangle is extracted as a feature vector with sex regressed out (Step 3), and leave-one-subject-out cross-validation (LOSO-CV) selects the λ yielding the highest R^2 (Step 4). In Step 5, the two cohort-specific lambdas (λ_1, λ_2) are averaged. Step 6 uses this mean λ for bidirectional cross-cohort prediction: a LASSO model trained on Cohort 1 is tested on Cohort 2 (yielding r_1, RMSE_1) and vice versa, with overall accuracy and root mean squared error (RMSE) computed as the mean across directions. In Step 7, statistical significance is assessed via permutation testing (10,000 iterations): training labels are shuffled within each cohort and Step 6 is repeated to generate a null distribution, with p-values calculated as the proportion of null accuracies $\geq$ observed accuracy. False discovery rate (FDR) correction (Benjamini–Hochberg) is then applied across all networks within each subscale. This procedure is repeated for each of the four IRI subscales (empathic concern, personal distress, fantasizing, perspective-taking) and each network or network combination tested.

2.6.6. Identification and Visualization of Top Beta Values

For each cross-cohort analysis, the beta coefficients from the LASSO models were stored and summed across models. To identify the most informative functional connections for predicting each behavioral measure, we examined the beta coefficients with the highest absolute values, as these represent the edges (i.e., connectivity values) with the greatest influence on the prediction, regardless of the direction of their effect. The top beta values were used to create the visualizations in Figures 3–5, which depict the most informative edges utilized by the LASSO models in the significant cross-cohort predictions of empathic concern, personal distress, fantasizing, and perspective-taking. The specific ROI pairs and their corresponding network affiliations for these top beta values are detailed in Supplemental Tables S2–S13.

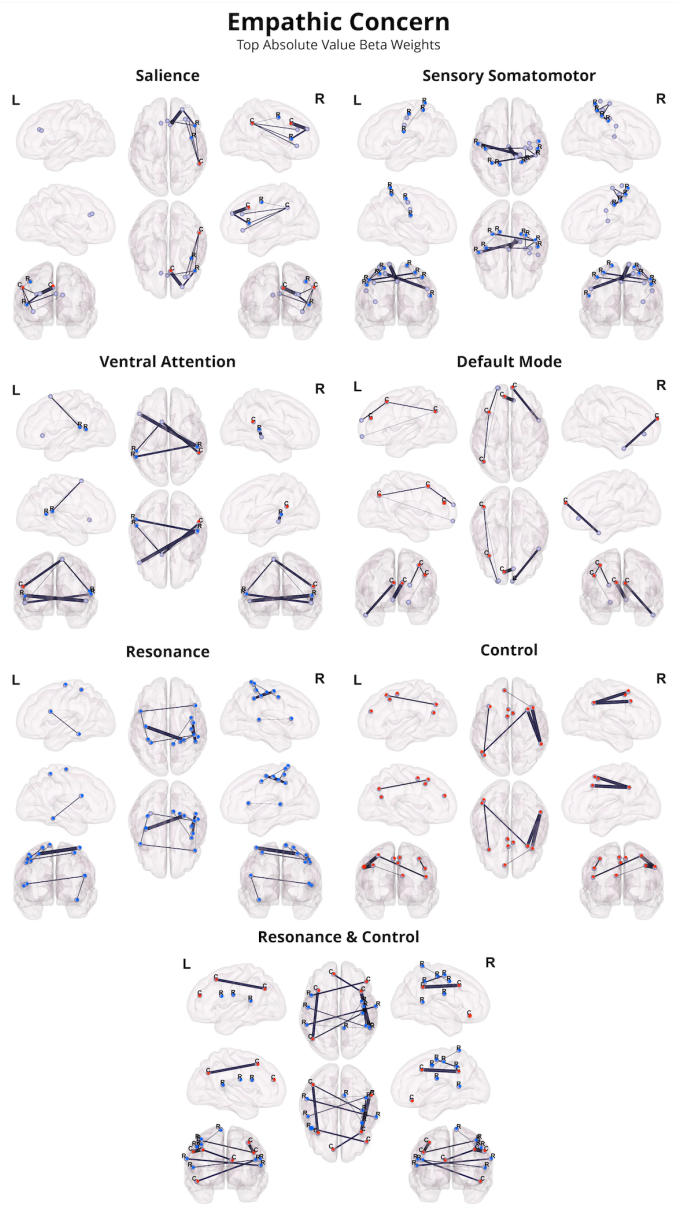

Figure 3. Most informative (i.e., highest absolute value betas) edges (i.e., connectivity values) utilized by the LASSO model in significant cross-cohort predictions of empathic concern. R (in blue) and C (in red) overlays on the nodes indicate membership in the resonance and control networks, respectively. These labels are not included when all nodes in a given network belong to either the resonance or control network, such as in the resonance network panel. The R and L labels indicate right and left hemispheres, respectively.

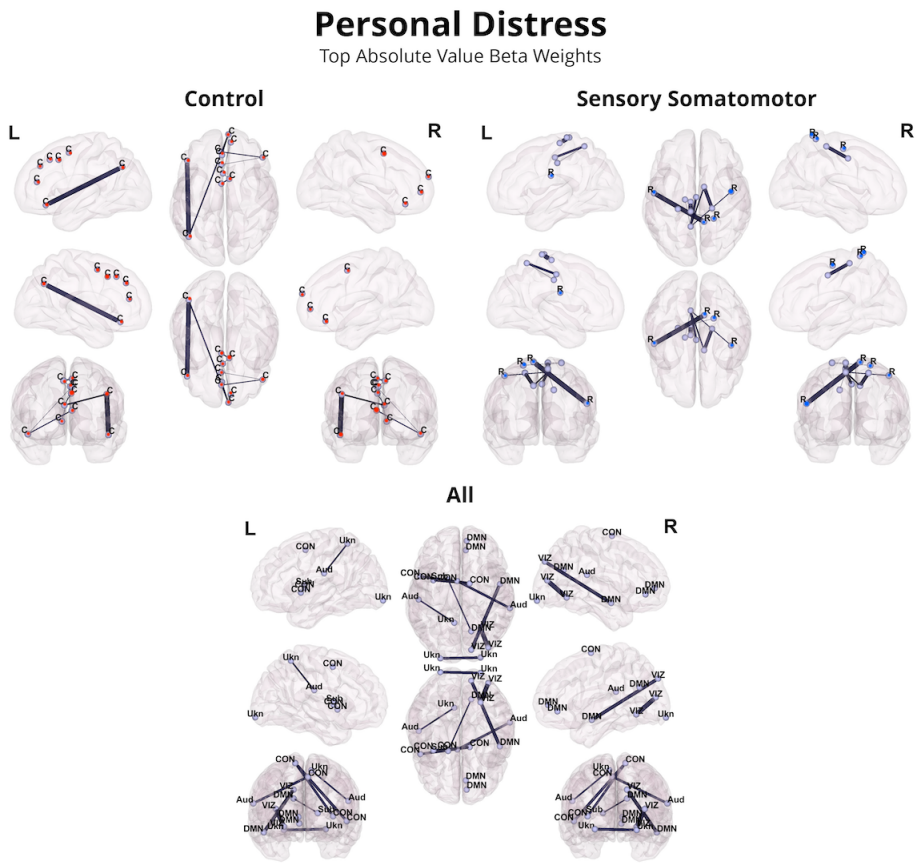

Figure 4. Most informative (i.e., highest absolute value betas) edges (i.e., connectivity values) utilized by the LASSO model in significant cross-cohort predictions of empathic concern. R (in blue) and C (in red) overlays on the nodes indicate membership in the resonance and control networks, respectively. These labels are not included when all nodes in a given network belong to either the resonance or control network, such as in the resonance network panel. Aud = auditory; CON = control; DMN = default mode network; Sub = subcortical; Ukn = unknown; VIZ = visual. The R and L labels indicate the right and left hemispheres, respectively.

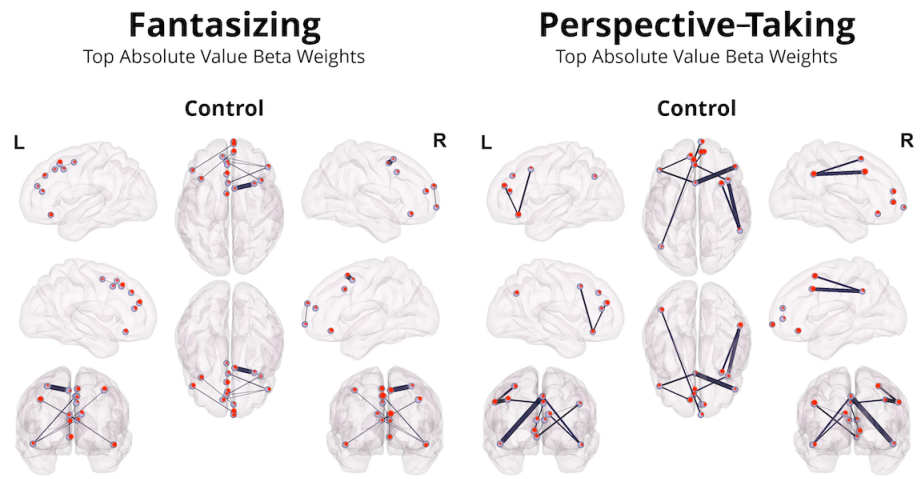

Figure 5. Most informative (i.e., highest absolute value betas) edges (i.e., connectivity values) utilized by the LASSO model in significant cross-cohort predictions of fantasizing (**left**) and perspective-taking (**right**). R (in blue) and C (in red) overlays on the nodes indicate membership in the resonance and control networks, respectively. The R and L labels indicate the right and left hemispheres, respectively.

2.6.7. Anatomical Mapping

To ensure maximal objectivity, anatomical labeling was conducted by harnessing meta-analytic data: ROI coordinates were taken from the power atlas and fed into the Neurosynth search engine (www.neurosynth.com). Associated anatomical labels for each X/Y/Z coordinate (indexed in MNI152 space) were aggregated into each description. Slight coordinate adjustments were noted in some cases upon input into Neurosynth.

3. Results

Results revealed several patterns and trends across the significant findings. The control network emerged as a consistent predictor of all four empathy subdimensions, with r-values ranging from 0.314 to 0.356, explaining 10.8% to 13% of the variance. Empathic concern was the most broadly predicted, with significant results observed in seven networks and r-values ranging from 0.281 to 0.451, explaining 8% to 20% of the variance (Figure 3, Table 1). Combined resonance and control network interactions predicted empathic concern to a greater extent than either network alone or the whole-brain "all" network.

Table 1. Descriptive statistics for Interpersonal Reactivity Index (IRI) subscale scores by cohort, with between-cohort comparisons (independent sample *t*-tests). Item-level responses were not retained, precluding computation of Cronbach's α; however, the IRI has demonstrated adequate internal consistency (α = 0.70–0.78) in prior validation work [5].

(a) Descriptive Statistics

IRI Subscale	Cohort	N	Mean	SD	Min	Max
Empathic Concern	Cohort 1	51	23.55	4.43	15.0	31.0
Empathic Concern	Cohort 2	45	19.82	3.51	12.0	28.0
Personal Distress	Cohort 1	51	14.18	6.05	2.0	27.0
Personal Distress	Cohort 2	45	12.53	4.10	2.0	22.0
Fantasizing	Cohort 1	51	19.67	5.05	8.0	34.0
Fantasizing	Cohort 2	45	18.73	4.91	5.0	28.0
Perspective-Taking	Cohort 1	51	20.47	4.99	6.0	29.0
Perspective-Taking	Cohort 2	45	19.40	4.35	11.0	28.0

(b) Between-Cohort Comparisons

IRI Subscale	*t*	df	*p*
Empathic Concern	4.53	94	<0.0001
Personal Distress	1.54	94	0.128
Fantasizing	0.92	94	0.362
Perspective-Taking	1.11	94	0.268

Descriptive statistics for each IRI subscale by cohort are reported in Table 1. Between-cohort comparisons revealed a significant difference in empathic concern ($t(94) = 4.53$, $p < 0.0001$), with Cohort 1 scoring higher ($M = 23.55$, $SD = 4.43$) than Cohort 2 ($M = 19.82$, $SD = 3.51$). No significant differences were observed for personal distress ($p = 0.128$), fantasizing ($p = 0.362$), or perspective-taking ($p = 0.268$). Notably, the significant cross-cohort prediction of empathetic concerns, despite this distributional shift, speaks to the generalizability of the model. Item-level responses were not retained, precluding the computation of Cronbach's α; however, the IRI has demonstrated adequate internal consistency ($\alpha = 0.70$–0.78) in prior validation work [5,79].

3.1. Empathic Concern

The Salience Network demonstrated the highest accuracy (FDR-corrected $p < 0.001$), followed by the Ventral Attention Network (FDR-corrected $p = 0.014$), and the combination of resonance and control networks (FDR-corrected $p = 0.01$). Significant predictions were also observed in the sensory somatomotor network (FDR-corrected $p = 0.012$), default mode network (FDR-corrected $p = 0.046$), resonance network alone (FDR-corrected $p = 0.01$), and control network alone (FDR-corrected $p = 0.012$) [20]. The default mode network showed a trend toward significance (FDR-corrected $p = 0.059$) (Figure 3, Table 2).

Table 2. Cross-cohort prediction accuracies, variance explained (R^2), root mean squared errors (RMSE), bootstrap confidence intervals (95% CI; 10,000 iterations), *p*-values obtained from permutation testing (10,000 iterations), and false discovery rate (FDR) corrected *p*-values for empathic concern using resting-state functional connectivity within various brain networks. Accuracy is represented by the Pearson correlation coefficient (*r*) between predicted and actual empathic concern scores. FDR correction applied within subscale using Benjamini–Hochberg. * $p < 0.05$, ** $p < 0.01$, *** $p < 0.005$. Significant results in **bold**.

Network	Accuracy (*r*)	R^2	RMSE	95% CI	*p*-Value	FDR *p*-Value
Visual	0.122	0.015	5.66	[−0.483; −0.120]	0.1441	0.1663
Salience	**0.451**	**0.205**	**5.93**	**[−0.384; −0.032]**	**0.0000**	**<0.0001** ***
Uncertain	0.009	0.001	7.11	[−0.473; −0.143]	0.4690	0.4690
Sensory Somatomotor	**0.281**	**0.080**	**6.05**	**[−0.355; 0.007]**	**0.0040**	**0.0120** *
Memory Retrieval	0.077	0.012	6.02	[−0.458; −0.083]	0.3072	0.3291
Ventral Attention	**0.354**	**0.125**	**5.53**	**[−0.408; −0.043]**	**0.0056**	**0.0140** *
Cingulo Opercular	0.205	0.046	6.04	[−0.400; −0.047]	0.0393	0.0737
Fronto Parietal	0.272	0.077	5.54	[−0.483; −0.143]	0.0899	0.1226
Default Mode	**0.309**	**0.096**	**5.27**	**[−0.371; −0.003]**	**0.0273**	**0.0585**
Dorsal Attention	0.130	0.018	13.52	[−0.175; 0.199]	0.1003	0.1254
Subcortical	0.225	0.052	5.67	[−0.445; −0.105]	0.0607	0.0911
Resonance	**0.337**	**0.119**	**5.46**	**[−0.362; −0.049]**	**0.0019**	**0.0095** **
Control	**0.356**	**0.130**	**5.58**	**[−0.297; 0.069]**	**0.0039**	**0.0120** *
Resonance & Control	**0.374**	**0.148**	**5.89**	**[−0.313; 0.041]**	**0.0016**	**0.0095** **
All	0.262	0.069	5.67	[−0.408; −0.076]	0.0498	0.0830

3.1.1. Salience

The analysis of the top connections within the Salience Network that are predictive of empathic concern revealed the following patterns. The temporoparietal junction (TPJ; ROI #204) appeared in four out of the eight top connections, connecting with the dorsolateral prefrontal cortex (DLPFC), Inferior Frontal/Anterior Cingulate (IF/AC), Premotor Cortex (PMC), and Ventrolateral Prefrontal Cortex/Anterior Insula (VLPFC/AI). The Anterior Cingulate Cortex (ACC) appeared in six out of the eight top connections, either alone or in combination with the Insula (INS), Dorsomedial Prefrontal Cortex (DMPFC), or Inferior Frontal Cortex (IFC). The IFC, in combination with the ACC (ROI #207), was connected to three different regions in the top connections. The DLPFC and the VLPFC, the latter in combination with the AI, were each connected to the TPJ. Out of the 11 unique ROIs involved in the top connections, three were affiliated with the control network, two were affiliated with the resonance network (Figure 3, Table S2).

3.1.2. Sensory Somatomotor

The analysis of the top connections within the sensory somatomotor network that are predictive of empathic concern revealed the following patterns. Inferior parietal lobule (IPL, ROI #255) appeared in four out of the ten top connections, connecting with the Somatosensory/Intraparietal Sulcus (SS/IPS), Middle Cingulate/Postcentral Gyrus/Superior Parietal/Posterior Insular (MC/PG/SP/PI), primary motor (PM), and Somatosensory (SS) regions. The supplementary motor/primary motor (SM/PM; ROI #19) was con-

nected to the supplementary motor/Primary Sensorimotor (SM/PS; ROI #15). The Precentral Gyrus/Somatosensory/Posterior Insula/Gyrus Superior (PG/SS/PI/GS; ROI #45) was connected to the Somatosensory Cortices/Superior Parietal/Sensorimotor Cortex (SSC/SP/SMC; ROI #38). The Motor Cortex (MC; ROI #44) was connected to the Posterior Insula (PI; ROI #43). The Secondary Somatosensory/Intraparietal (SSS/IP; ROI #25) was connected to the primary motor (PM; ROI #21). The Sensorimotor Cortex (SMC; ROI #41) was connected to the PM (ROI #21). The primary motor/Somatosensory (PM/SS; ROI #28) was connected to the Premotor Cortex/primary motor (PMC/PM; ROI #42). Out of the 16 unique ROIs involved in the top connections, seven were affiliated with the resonance network (Figure 3, Table S3).

3.1.3. Ventral Attention

The analysis of the top connections within the Ventral Attention Network that are predictive of empathic concern revealed the following patterns. The supplementary motor/temporoparietal junction (SM/TPJ; ROI #138) appeared in four out of the eight top connections, connecting with the Temporoparietal (TP; ROI #235), Superior Temporal/Planum Temporale (ST/PT; ROI #237), Posterior Superior/Superior Temporal (PS/ST; ROI #236), and Superior Temporal/Temporal Sulcus/Temporal Gyrus (ST/TS/TG; ROI #239) regions. The ST/TS/TG (ROI #239) was connected to the PS/ST (ROI #236) and the Superior Temporal/Auditory Cortex/Temporal Sulcus (ST/AC/TS; ROI #238). The Inferior Frontal (IF; ROI #242) was connected to the ST/AC/TS (ROI #238). Out of the eight unique ROIs involved in the top connections, four were affiliated with the resonance network, and one was affiliated with the control network (Figure 3, Table S4).

3.1.4. Default Mode

The analysis of the top connections within the default mode network that are predictive of empathic concern revealed the following patterns. The angular gyrus/Lateral Parietal/Posterior Cingulate (AG/LP/PC; ROI #86) appeared in two of the six top connections, connecting with the Gyrus Precuneus (GP; ROI #78) and the dorsolateral prefrontal cortex (DLPFC; ROI #100). The DLPFC (ROI #100) was also connected to the Anterior Hippocampus/accumbens (AH/AC; ROI #114). The Anterior Temporal (AT; ROI #128) was connected to the Dorsomedial Prefrontal (DMP; ROI #106). The medial prefrontal cortex (MPFC; ROI #115) was connected to the Anterior Cingulate/Medial Prefrontal/Ventral Striatum (AC/MP/VS; ROI #110). Out of the nine unique ROIs involved in the top connections, four were affiliated with the control network, while the remaining five were not assigned to a specific network (Figure 3, Table S5).

3.1.5. Resonance

The analysis of the top connections within the resonance network that are predictive of empathic concern revealed the following patterns. The Inferior Frontal (IF; ROI #176) appeared in two of the ten top connections, connecting with the Inferior Frontal/Anterior Cingulate (IF/AC; ROI #207) and the Parahippocampal Cortex/Medial Temporal (PC/MT; ROI #126). Inferior parietal lobule (IPL, ROI #255) appeared in two of the top connections, connecting with the Somatosensory Cortex/Intraparietal Sulcus (SC/IS; ROI #30) and the Middle Cingulate/Postcentral Gyrus/Superior Parietal/Posterior Insular (MC/PG/SP/PI; ROI #32). The IF/AC (ROI #207) was also connected to the Superior Temporal/Auditory Cortex/Temporal Sulcus (ST/AC/TS; ROI #238). The Premotor Cortex (PMC; ROI #205) was connected to the Superior Parietal (SP; ROI #22). The Inferior Parietal/Intraparietal Sulcus (IP/IS; ROI #190) was connected to the primary motor (PM; ROI #36) and the Motor Cortex/Premotor Cortex (MC/PMC; ROI #29). The Secondary Somatosensory/Intraparietal (SSS/IP; ROI #25) was connected to primary cortex (ROI #37). Out of the 17 network-

affiliated ROIs in this dataset, nine were affiliated with the Sensory/Somatomotor Hand Network, four were affiliated with the Salience Network, three were affiliated with the Fronto-parietal Task control network, and one was affiliated with the Ventral Attention Network (Figure 3, Table S6).

3.1.6. Control

The analysis of the top connections within the control network that are predictive of empathic concern revealed the following patterns. The supplementary motor (SM; ROI #54) appeared in two of the eight top connections, connecting with the supplementary motor/Premotor Cortex (SM/PMC; ROI #47) and the Parietal Cortex/Medial Frontal (PC/MF; ROI #213). The TPJ (ROI #204) also appeared in two of the top connections, connecting with the Prefrontal/Parietal (PP; ROI #193) and the Fronto Parietal (FP; ROI #196). The medial prefrontal cortex (MPFC; ROI #115) was connected to the FP (ROI #196). The angular gyrus/Lateral Parietal/Posterior Cingulate (AG/LP/PC; ROI #86) was connected to the dorsolateral prefrontal cortex (DLPFC; ROI #100). The Temporo Parietal/angular gyrus (TP/AG; ROI #79) was connected to the PP (ROI #193). Out of the 14 network-affiliated ROIs in this dataset, four were affiliated with the default mode network (DMN), three were affiliated with the Fronto-parietal Task control network, three were affiliated with the Cingulo-opercular Task control network, and three were affiliated with the Salience Network (Figure 3, Table S7).

3.1.7. Resonance and Control

The analysis of the top connections within the combined resonance and control networks that are predictive of empathic concern revealed the following patterns. The Superior Temporal/Planum Temporale (ST/PT; ROI #237) appeared in two of the ten top connections, connecting with the Postcentral Gyrus/Somatosensory Cortices (PG/SC; ROI #46) and the Temporal Sulcus/Posterior Superior/Superior Temporal (TS/PS/ST; ROI #240). The angular gyrus/Lateral Parietal/Posterior Cingulate (AG/LP/PC; ROI #86) also appeared in two of the top connections, connecting with the primary motor (PM; ROI #36) and the dorsolateral prefrontal cortex (DLPFC; ROI #100). The Fronto Parietal (FP; ROI #196) was connected to the medial prefrontal cortex (MPFC; ROI #115) and the Inferior Parietal/Frontal Gyrus (TPJ; ROI #204). The Inferior Frontal (IF; ROI #176) was connected to the Lateral Orbitofrontal (LO; ROI #139). The Premotor Cortex (PMC; ROI #205) was connected to the Superior Parietal (SP; ROI #22). The Precentral Gyrus/Somatosensory/Posterior Insula/Gyrus Superior (PG/SS/PI/GS; ROI #45) was connected to the TS/PS/ST (ROI #240). The Inferior Parietal/Intraparietal Sulcus (IP/IS; ROI #190) was connected to the Motor Cortex/Premotor Cortex (MC/PMC; ROI #29). Out of the 18 network-affiliated ROIs in this dataset, five (27.8%) were affiliated with the default mode network (DMN), four (22.2%) were affiliated with the Fronto-parietal Task control network, four were affiliated with the Ventral Attention Network (VAtt), three were affiliated with the Sensory/Somatomotor Networks (two Hand/one Mouth), and two were affiliated with the Salience Network (Figure 3, Table S8).

Examining analyses of the top connections in multiple networks predictive of empathic concern, three high-level insights emerge. First, edges involving the Inferior Parietal/Frontal Gyrus (TPJ) contributed most strongly to predictions across the Salience, control, and combined resonance/control networks. Second, the Anterior Cingulate Cortex (ACC) and its connections with the Inferior Frontal (IF) regions are prominent within the Salience Network. Finally, the default mode network (DMN) regions, such as the angular gyrus/Lateral Parietal/Posterior Cingulate (AG/LP/PC) and the dorsolateral

prefrontal cortex (DLPFC), are consistently connected across the control and combined resonance/control networks.

To examine the specific ROI pairs and their corresponding network affiliations for the top beta values (i.e., the most informative edges) in the significant cross-cohort predictions of empathic concern, please refer to Supplemental Tables S2–S8. These tables provide detailed information on the top magnitude beta values for each network or network combination that successfully predicted empathic concern, including the Salience Network (Table S2), sensory somatomotor network (Table S3), Ventral Attention Network (Table S4), default mode network (Table S5), resonance network (Table S6), control network (Table S7), and the combined resonance and control networks (Table S8).

3.2. Personal Distress

Significant predictions were observed in the sensory somatomotor network (FDR-corrected $p = 0.025$), control network (FDR-corrected $p = 0.025$), and the combination of all networks (FDR-corrected $p = 0.025$) (Figure 4, Table 3).

Table 3. Cross-cohort prediction accuracies for personal distress. Conventions as in Table 2.

Network	Accuracy (*r*)	R^2	RMSE	95% CI	*p*-Value	FDR *p*-Value
Visual	−0.038	0.003	6.81	[−0.305; 0.033]	0.6088	0.6617
Salience	−0.025	0.003	7.53	[−0.227; 0.150]	0.5979	0.6617
Uncertain	0.110	0.015	7.97	[−0.027; 0.317]	0.1509	0.2515
Sensory Somatomotor	**0.285**	**0.087**	**5.14**	**[0.018; 0.364]**	**0.0054**	**0.0270** *
Memory Retrieval	0.192	0.039	5.51	[−0.197; 0.175]	0.0616	0.1320
Ventral Attention	−0.036	0.008	5.72	[−0.287; 0.155]	0.6176	0.6617
Cingulo Opercular	−0.105	0.011	10.18	[−0.258; 0.124]	0.8322	0.8322
Fronto Parietal	0.195	0.053	6.68	[−0.084; 0.334]	0.0522	0.1305
Default Mode	0.276	0.076	5.01	[0.066; 0.397]	0.0231	0.0866
Dorsal Attention	0.144	0.027	5.77	[−0.200; 0.190]	0.1889	0.2834
Subcortical	0.020	0.012	5.80	[−0.288; 0.117]	0.4428	0.6038
Resonance	0.139	0.038	6.15	[−0.155; 0.219]	0.1247	0.2338
Control	**0.329**	**0.108**	**4.99**	**[0.092; 0.455]**	**0.0028**	**0.0270** *
All	**0.298**	**0.092**	**5.31**	**[−0.071; 0.319]**	**0.0043**	**0.0270** *
Resonance & Control	0.213	0.046	5.32	[−0.066; 0.300]	0.0477	0.1305

3.2.1. Sensory Somatomotor

The analysis of the top connections within the sensory somatomotor network that are predictive of personal distress revealed the following patterns. The Parieto Occipital/accumbens (PO/AC; ROI #13) appeared in five out of the nine top connections, connecting with the supplementary motor/Primary Sensorimotor (SM/PS; ROI #15), primary motor/supplementary motor (PM/SM; ROI #16), Ventral Promotor (VP; ROI #14), Motor Cortex/Premotor Cortex (MC/PMC; ROI #29), and Somatosensory/primary motor (SS/PM; ROI #28). The supplementary motor (SM) regions, either alone or in combination with other regions such as the Primary Sensorimotor, primary motor, or accumbens, appeared in four of the top connections (ROI #15, 16, 17, 23). The Middle Cingulate/Postcentral Gyrus/Superior Parietal/Posterior Insular (MC/PG/SP/PI; ROI #32) was connected to the Somatosensory Cortex/primary motor/supplementary motor/accumbens (SC/PM/SM/AC; ROI #23). The primary motor (PM) regions, either alone or in combination with other regions such as the Somatosensory or supplementary motor, appeared in three of the top connections (ROI #16, 18, 28). The Precentral Gyrus/Somatosensory/Posterior Insula/Gyrus Superior (PG/SS/PI/GS; ROI #45) was connected to the Superior Parietal (SP; ROI #22). Out of the 11 unique ROIs involved in the top connections, three were affiliated with the resonance network (Figure 4, Table S9).

3.2.2. Control

The analysis of the top connections within the control network that are predictive of personal distress revealed the following patterns. The supplementary motor (SM; ROI #54) appeared in two of the eight top connections, connecting with the supplementary motor/Premotor Cortex (SM/PMC; ROI #47) and the Parietal Cortex/Medial Frontal (PC/MF; ROI #213). The angular gyrus/Lateral Parietal/Posterior Cingulate (AG/LP/PC; ROI #86) also appeared in two of the top connections, connecting with the Dorsomedial Prefrontal (DMP; ROI #106) and the Inferior Frontal (IF; ROI #137). The Lateral Orbitofrontal (LO; ROI #139) was connected to the Anterior Prefrontal/Medial Lateral/Inferior Frontal (AP/ML/IF; ROI #202) and the Anterior Cingulate/medial prefrontal (AC/MP; ROI #113). The medial prefrontal (MP; ROI #112) was connected to the DMP (ROI #106). The medial prefrontal/Anterior Cingulate (MP/AC; ROI #108) was connected to the PC/MF (ROI #213). Out of the 16 network-affiliated ROIs in this dataset, 12 were affiliated with the default mode network (DMN), two were affiliated with the Cingulo-opercular Task control network, one was affiliated with the Salience Network, and one was affiliated with the Fronto-parietal Task control network (Figure 4, Table S10).

3.2.3. All

The analysis of the top connections across all networks that are predictive of personal distress revealed the following patterns. The Primary/supplementary motor (P/SM; ROI #53) appeared in two of the nine top connections, connecting with the supplementary motor/Premotor Cortex/primary motor (SM/PMC/PM; ROI #58) and the Parieto Occipital/accumbens (PO/AC; ROI #156). The accumbens (AC) regions, either alone or in combination with other regions such as the Inferior Occipital, Parieto Occipital, or Ventral Visual/Occipital Temporal/Fusiform Gyrus/Amygdala Anterior, appeared in three of the top connections (ROI #1, 2, 150). The medial prefrontal/Anterior Cingulate (MP/AC; ROI #108) was connected to the Anterior Cingulate/medial prefrontal/Ventral Striatum (AC/MP/VS; ROI #110). The basal ganglia/Striatum/Caudate (BG/ST/CA; ROI #228) was connected to the Precuneus/Ventral Tegmental/Medial Temporal (PC/VT/MT; ROI #93). The Secondary Somatosensory/Primary Somatosensory (SS/PS; ROI #69) was connected to the Parieto Occipital/accumbens (PO/AC; ROI #13). The Posterior Insula/Anterior Insula/basal ganglia/Somatosensory Cortex (PI/AI/BG/SC; ROI #57) was connected to the P/SM (ROI #53). The Premotor Cortex (PMC; ROI #62) was connected to the supplementary motor/Premotor Cortex (SM/PMC; ROI #47). The Occipitotemporal (OT; ROI #169) was connected to MPFC (ROI #123). Out of the 16 network-affiliated ROIs in this dataset, five were affiliated with the Cingulo-opercular Task control network, three were affiliated with the Visual Network, three were affiliated with the default mode network (DMN), two were affiliated with the Auditory Network, one was affiliated with the Sensory/Somatomotor Hand Network, one was affiliated with the Subcortical Network, and one was affiliated with the control network (Figure 4, Table S11). Across multiple networks, personal distress was predicted by patterns of connectivity with sensorimotor integration areas (especially supplementary/primary motor), cognitive control regions (medial prefrontal, angular gyrus), default mode areas, and subcortical regions (accumbens, basal ganglia) across the different network analyses. The parieto-occipital/accumbens region emerged as a potential key hub within the sensory somatomotor network.

3.3. Fantasizing

Fantasizing was significantly predicted only by the control network (FDR-corrected $p = 0.004$, $p = 0.004$, $p = 0.004$) (Figure 5, Table 4).

Table 4. Cross-cohort prediction accuracies for fantasizing. Conventions as in Table 2.

Network	Accuracy (r)	R^2	RMSE	95% CI	p-Value	FDR p-Value
Visual	0.165	0.027	5.57	[−0.027; 0.249]	0.0833	0.1970
Salience	0.125	0.019	7.93	[−0.047; 0.318]	0.1487	0.2231
Uncertain	0.072	0.012	5.69	[−0.078; 0.240]	0.2654	0.3318
Sensory Somatomotor	0.134	0.019	5.25	[−0.088; 0.302]	0.1032	0.1970
Memory Retrieval	0.190	0.040	5.09	[−0.071; 0.301]	0.0680	0.1970
Ventral Attention	0.317	0.107	4.77	[0.112; 0.476]	0.0070	0.0525
Cingulo Opercular	0.222	0.065	5.26	[−0.097; 0.278]	0.0281	0.1405
Fronto Parietal	0.147	0.024	5.33	[−0.090; 0.329]	0.0883	0.1970
Default Mode	0.058	0.022	5.50	[−0.113; 0.293]	0.3026	0.3492
Dorsal Attention	0.068	0.008	5.50	[−0.220; 0.193]	0.2453	0.3318
Subcortical	0.054	0.003	5.52	[−0.134; 0.242]	0.3501	0.3751
Resonance	−0.058	0.003	6.55	[−0.294; 0.159]	0.6989	0.6989
Control	**0.343**	**0.118**	**5.91**	**[0.143; 0.506]**	**0.0005**	**0.0075** **
All	0.148	0.024	5.26	[−0.063; 0.306]	0.1182	0.1970
Resonance & Control	0.146	0.021	5.08	[−0.082; 0.325]	0.1136	0.1970

Control

The analysis of the top connections within the control network that are predictive of fantasizing revealed the following patterns. The Lateral Orbitofrontal (LO; ROI #139) appeared in three of the ten top connections, connecting with the Parietal Cortex/Medial Frontal (PC/MF; ROI #213), the medial prefrontal cortex (MPFC; ROI #115), and the Anterior Cingulate/medial prefrontal (AC/MP; ROI #113). The Dorsomedial Prefrontal (DMP; ROI #106) also appeared in three of the top connections, connecting with the accumbens (AC; ROI #75), secondary somatosensory cortex (SII, ROI #105), and the Inferior Frontal (IF; ROI #137). The supplementary motor (SM; ROI #54) was connected to the Prefrontal/Parietal (PP; ROI #193) and the Anterior Prefrontal/Medial Lateral/Inferior Frontal (AP/ML/IF; ROI #202). The Fronto Parietal (FP; ROI #196) was connected to the AC/MP (ROI #113). The dorsolateral prefrontal cortex (DLPFC; ROI #100) was connected to an unknown region (ROI #105). The medial prefrontal (MP; ROI #112) was connected to SII (ROI #105). The supplementary motor/Premotor Cortex (SM/PMC; ROI #47) was connected to the AP/ML/IF (ROI #202). Out of the 18 network-affiliated ROIs in this dataset, 12 were affiliated with the default mode network (DMN), three were affiliated with the Fronto-parietal Task control network, two were affiliated with the Cingulo-opercular Task control network, and one was affiliated with the Salience Network (Figure 5, Table S12).

3.4. Perspective-Taking

Perspective-taking was significantly predicted by the control network (FDR-corrected $p = 0.003$) (Figure 5, Table 5).

Control

The analysis of the top connections within the control network that are predictive of perspective-taking revealed the following patterns. The Parietal Cortex/Medial Frontal (PC/MF; ROI #213) appeared in two of the ten top connections, connecting with the Lateral Orbitofrontal (LO; ROI #139) and the Inferior Frontal (IF; ROI #137). The medial prefrontal (MP; ROI #112) also appeared in two of the top connections, connecting with the Fronto Parietal (FP; ROI #196) and the medial prefrontal/Anterior Cingulate (MP/AC; ROI #108). The accumbens (AC; ROI #75) was connected to the Anterior Cingulate/medial prefrontal (AC/MP; ROI #113) and the angular gyrus/Lateral Parietal/Posterior Cingulate (AG/LP/PC; ROI #86). The IF (ROI #137) was connected to the medial prefrontal cortex (MPFC; ROI #115). The AG/LP/PC (ROI #86) was connected to an unknown region (ROI #105). The Inferior Parietal/Frontal Gyrus (TPJ; ROI #204) appeared in two of the top connections, connecting with the Prefrontal/Parietal (PP; ROI #193) and the FP (ROI #196).

Out of the 18 network-affiliated ROIs in this dataset, 12 were affiliated with the default mode network (DMN), three were affiliated with the Fronto-parietal Task control network, two were affiliated with the Cingulo-opercular Task control network, and one was affiliated with the Salience Network (Figure 5, Table S13).

Table 5. Cross-cohort prediction accuracies for perspective-taking. Conventions as in Table 2.

Network	Accuracy (r)	R^2	RMSE	95% CI	p-Value	FDR p-Value
Visual	0.083	0.012	6.49	[−0.112; 0.304]	0.2091	0.5513
Salience	−0.087	0.010	6.41	[−0.284; 0.102]	0.7723	0.8527
Uncertain	0.041	0.002	6.89	[−0.168; 0.234]	0.3525	0.5875
Sensory Somatomotor	0.154	0.027	5.61	[−0.199; 0.301]	0.0337	0.1264
Memory Retrieval	0.075	0.007	5.15	[−0.188; 0.195]	0.2582	0.5533
Ventral Attention	0.063	0.005	5.07	[−0.222; 0.285]	0.2964	0.5558
Cingulo Opercular	0.089	0.008	5.17	[−0.190; 0.177]	0.2205	0.5513
Fronto Parietal	−0.108	0.015	5.45	[−0.342; 0.055]	0.8527	0.8527
Default Mode	0.216	0.053	4.97	[−0.030; 0.371]	0.0276	0.1264
Dorsal Attention	−0.018	0.007	17.92	[−0.245; 0.208]	0.5722	0.8482
Subcortical	−0.106	0.020	5.58	[−0.279; 0.098]	0.8378	0.8527
Resonance	−0.032	0.040	5.98	[−0.261; 0.128]	0.6220	0.8482
Control	**0.314**	**0.120**	**5.35**	**[−0.092; 0.371]**	**0.0009**	**0.0135** *
All	−0.086	0.011	5.00	[−0.352; 0.074]	0.7668	0.8527
Resonance & Control	0.209	0.075	5.51	[−0.119; 0.299]	0.0210	0.1264

3.5. Model Complexity and Feature Stability

To assess model complexity and feature selection stability across cross-cohort directions, we report the number of non-zero LASSO coefficients for each significant prediction in Table 6. LASSO regularization substantially reduced dimensionality across all models, with the number of non-zero coefficients ranging from three to 39 out of up to 34,716 possible features. Overlap between features selected in each cross-cohort direction was generally low (0–14.3%), indicating that while the models achieve comparable predictive accuracy in both directions, they rely on partially distinct sets of edges to do so. This is consistent with the LASSO's known behavior under multicollinearity, where multiple correlated features may be interchangeably selected without compromising prediction.

Table 6. Model complexity and feature stability for significant cross-cohort predictions. Total Features = number of functional connectivity edges entering the model. Non-Zero coefficients reported separately for each cross-cohort direction (A→B = train Cohort 1, test Cohort 2; B→A = train Cohort 2, test Cohort 1). Overlap = edges with non-zero coefficients in both directions. Overlap % = overlap count relative to the union of non-zero edges.

Subscale	Network	Total Features	Non-Zero (A→B)	Non-Zero (B→A)	Overlap	Overlap %
EC	Salience	153	4	4	1	14.3%
EC	Sensory Somatomotor	595	35	19	0	0.0%
EC	Ventral Attention	36	3	7	1	11.1%
EC	Resonance	561	9	9	0	0.0%
EC	Control	231	13	7	0	0.0%
EC	Resonance & Control	1540	24	16	0	0.0%
PD	Sensory Somatomotor	595	13	8	0	0.0%
PD	Control	231	15	11	2	8.3%
PD	All	34,716	23	18	0	0.0%
FS	Control	231	39	34	4	5.8%
PT	Control	231	22	18	5	14.3%

4. Discussion

We robustly replicated and extended the results in Christov-Moore et al. [76]. rsFC within a priori resonance and control networks were more broadly informative for pre-

dicting individual differences in empathic function than canonical resting-state networks. The control network emerged as a consistent predictor across all four subdimensions (r-values ranging from 0.314 to 0.356, explaining 9.9% to 12.7% of the variance), suggesting its central role in empathic processing.

Empathic concern showed the most robust set of findings, with significant predictions observed in seven different networks or network combinations (r-values ranging from 0.281 to 0.451, explaining 8% to 20.5% of the variance), highlighting the complex nature of this particular subdimension. In agreement with past findings [2,24], empathic concern seems to be subserved by characteristic interactions between resonance and control networks. Edges involving the inferior parietal lobule/frontal gyrus contributed most strongly to predictions across salience, control, and resonance/control networks.

Evidence suggests that the more complex a given psychological process is, the more likely it is to engage the cooperation of several brain regions [67], suggesting empathic concern may be the most integrative and complex of empathy's subdimensions. It is important to mention, however, that this subdimension measures feelings of sympathy and compassion and may be easier to answer as participants have likely developed and considered these traits already. This may position empathetic concern, both as a marker for global brain health as well as a benchmark to observe dysfunction and return to normal function following an intervention.

Personal distress (PD) was the only subdimension predicted by the "all" network, potentially speaking to the individual differences in global upregulation of arousal driving (or driven) by the emphasis on personal aversive responses to others. Interestingly, PD is an earlier process and seen more often in children, while EC is a more refined and complex function, associated with maturity.

Perspective-taking was primarily reflected in patterns of connectivity between cortical midline areas like the medial prefrontal and parietal cortices, as well as lateral prefrontal and parietal regions implicated in cognitive control and attentional processes. The involvement of the accumbens and default mode areas suggests roles for reward and self-referential mechanisms as well in perspective-taking ability.

Perhaps effective control of vicarious somatosensation is key here, and patterns of attention orientation interact with this dimension. Indeed, developmental and behavioral/psychophysiological data suggest that the variations in personal distress, and its relation to sympathy, revolve around attention and self-regulation of vicarious responses to others' pain and distress [93–95].

Fantasizing was predicted by connectivity patterns primarily involving lateral and medial prefrontal regions, along with the supplementary motor area. These cortical midline areas serve roles in cognitive control, self-referential processing, and memory retrieval—functions that may underlie the cognitive aspects of fantasizing. Many of these regions are a part of the default mode network and contribute to the ability to fantasize in these empathic scenarios.

Finally, the feature dimensionality results reported in Table 6 further support the utility of theory-driven network selection. Despite having access to 34,716 possible edges, the "All" network only achieved significant prediction for personal distress, and with lower accuracy (r = 0.298) than the control network alone (r = 0.329, 231 features). For empathetic concern, the combined resonance and control network (1540 features) outperformed the "All" network (r = 0.374 vs. 0.262), which did not survive FDR correction. LASSO regularization reduced all models to comparable numbers of non-zero coefficients (3–39 regardless of input dimensionality), suggesting that the advantage of theory-driven networks lies not in regularization behavior but in providing a more informative feature space—one in which a greater proportion of edges carry signal relevant to the construct of interest.

This supports the broader argument that a priori task-derived networks can help constrain resting-state analyses by concentrating predictive information and reducing noise from irrelevant connections.

While examining sex interactions within the current cross-cohort method by comparing model performance between segregated cohorts (∼25 per training and testing group) would be difficult to achieve while maintaining robustness and generalizability, future studies with sufficiently large cohorts should examine sex interactions with connectivity-empathy interactions [58], due to the many robust sex differences observed in empathic dispositions [96].

5. Conclusions

Here we extend the results from our 2020 study by replicating our findings in a far more robust, generalizable, cross-cohort approach. In contemporary neuroscience the need for multiple pipelines [97,98] and replication studies [99–101] has become increasingly highlighted, particularly for findings intended for eventual clinical application. Cross-cohort, high sample predictive studies of this kind are necessary given contemporary concerns around lack of replicability or generalizability of the findings of prognostic neuroscience [77].

Our multivariate approach, which is able to leverage patterns of information with minimal prior assumptions, lends novel information about subfacets of empathic function. The number and extent of networks implicated suggest that empathic concern, for example, emerges from a wider set of subsystems in tandem, and hence may be more affected by global psychopathology and a good marker for healthy, integrated brain function. Conversely, these findings suggest that personal distress may be largely a function of attentional systems, consistent with its earlier role in the evolutionary development of empathy.

Our results also demonstrate that theory-driven networks achieve equal or superior predictive accuracy to whole-brain approaches despite containing orders of magnitude fewer features, with LASSO reducing all models to comparable numbers of non-zero coefficients regardless of input dimensionality. This suggests that the advantage of a priori network selection lies in concentrating predictive signal rather than relying on regularization to filter noise from large feature spaces, reinforcing the value of targeted, hypothesis-driven approaches in resting-state predictive neuroscience.

Finally, we are making our model and datasets publicly available, and hope that other groups can lend similar datasets towards further validating and improving this model. This may eventually be leveraged to dissect empathic subcomponents in populations for whom traditional questionnaires and scanner tasks are difficult or impossible. This approach may provide a model for the rigorous, generalizable use of task-defined networks in resting-state data to investigate other domains of human cognition beyond empathy.

Supplementary Materials: The following supporting information can be downloaded at: https://www.mdpi.com/article/10.3390/neuroimaging1030011/s1, Table S1: MNI coordinates of Powers cortical atlas ROI's employed in resonance and control networks. IFGpo = Inferior Frontal Gyrus pars opercularis. Table S2: Top magnitude beta values for the Salience Network most informative in predicting empathic concern in the cross-cohort analysis, including ROI pairs and network affiliations. Table S3: Top magnitude beta values for the Sensory Somatomotor Network most informative in predicting empathic concern across cohorts, including ROI pairs and network affiliations. Table S4: Top magnitude beta values for the Ventral Attention Network most informative in predicting empathic concern in the cross-cohort analysis, including ROI pairs and network affiliations. Table S5: Top magnitude beta values for the Default Mode Network most informative in predicting empathic concern across cohorts, including ROI pairs and network affiliations. Table S6: Top magnitude beta values for the Resonance Network most informative in predicting empathic concern in the

cross-cohort analysis, including ROI pairs and network affiliations. Table S7: Top magnitude beta values for the Control Network most informative in predicting empathic concern across cohorts, including ROI pairs and network affiliations. Table S8: Top magnitude beta values for the combined Resonance and Control Networks most informative in predicting empathic concern in the cross-cohort analysis, including ROI pairs and network affiliations. Table S9: Top magnitude beta values for the Sensory Somatomotor Network most informative in predicting personal distress across cohorts, including ROI pairs and network affiliations. Table S10: Top magnitude beta values for the Control Network most informative in predicting personal distress in the cross-cohort analysis, including ROI pairs and network affiliations. Table S11: Top magnitude beta values most informative in predicting personal distress across cohorts when using ROIs from all networks (including the bilateral amygdala), including ROI pairs and network affiliations. Table S12: Top magnitude beta values for the Control Network most informative in predicting fantasizing in the cross-cohort analysis, including ROI pairs and network affiliations. Table S13: Top magnitude beta values for the Control Network most informative in predicting perspective-taking across cohorts, including ROI pairs and network affiliations.

Author Contributions: Conceptualization, N.R. and L.C.-M.; methodology, N.R.; software, N.R.; validation, N.R., R.L., T.D., J.K., M.I. and L.C.-M.; formal analysis, N.R.; investigation, N.R. and L.C.-M.; resources, J.K. and M.I.; data curation, N.R. and L.C.-M.; writing—original draft preparation, N.R. and L.C.-M.; writing—review and editing, R.L., T.D., J.K. and M.I.; visualization, N.R.; supervision, L.C.-M., J.K. and M.I.; project administration, N.R. and L.C.-M.; funding acquisition, N.R. and J.K. All authors have read and agreed to the published version of the manuscript.

Funding: This work was supported by a grant from Tiny Blue Dot Foundation to N.R., and from Templeton World Charity Foundation (TWCF0334) to J.K.

Institutional Review Board Statement: The study was conducted in accordance with the Declaration of Helsinki, and approved by the Institutional Review Board of UCLA.

Informed Consent Statement: Informed consent was obtained from all subjects involved in the study.

Data Availability Statement: All data is freely available upon request. The data presented in this study will be openly available in OSF.io at https://osf.io/ukemb (accessed on 25 November 2025). All analysis scripts—including preprocessing, cross-cohort LASSO prediction, permutation testing, confidence interval estimation, and feature stability extraction—are publicly available at https://github.com/Institute-for-Advanced-Consciousness/Reggente-2026-CrossCohort-Prediction-Empathy (accessed on 9 April 2026).

Acknowledgments: We thank all participants for their time and contribution to this research.

Conflicts of Interest: The authors declare no conflicts of interest. The funders had no role in the design of the study; in the collection, analyses, or interpretation of data; in the writing of the manuscript; or in the decision to publish the results.

Abbreviations

The following abbreviations are used in this manuscript:

ACC	Anterior Cingulate Cortex
DLPFC	Dorsolateral Prefrontal Cortex
DMN	Default Mode Network
EC	Empathic Concern
FDR	False Discovery Rate
fMRI	Functional Magnetic Resonance Imaging
FS	Fantasizing Scale
IRI	Interpersonal Reactivity Index
LASSO	Least Absolute Shrinkage and Selection Operator

PD	Personal Distress
PT	Perspective-Taking
ROI	Region of Interest
rsFC	Resting-State Functional Connectivity
TPJ	Temporoparietal Junction

References

1. Bartochowski, Z.; Gatla, S.; Khoury, R.; Al-Dahhak, R.; Grossberg, G.T. Empathy changes in neurocognitive disorders: A review. *Ann. Clin. Psychiatry* **2018**, *30*, 220–232. [CrossRef] [PubMed]
2. Christov-Moore, L.; Iacoboni, M. Self-other resonance, its control and prosocial inclinations: Brain-behavior relationships. *Hum. Brain Mapp.* **2016**, *37*, 1544–1558. [CrossRef] [PubMed]
3. Decety, J.; Jackson, P.L. A Social-Neuroscience Perspective on Empathy. *Curr. Dir. Psychol. Sci.* **2006**, *15*, 54–58. [CrossRef]
4. Zaki, J.; Ochsner, K. The neuroscience of empathy: Progress, pitfalls and promise. *Nat. Neurosci.* **2012**, *15*, 675–680. [CrossRef]
5. Davis, M.H. Measuring Individual Differences in Empathy: Evidence for a Multidimensional Approach. *J. Personal. Soc. Psychol.* **1983**, *44*, 113–126. [CrossRef]
6. Preston, S.D.; de Waal, F.B.M. Empathy: Its ultimate and proximate bases. *Behav. Brain Sci.* **2002**, *25*, 1–20. [CrossRef]
7. Smith, A. Cognitive Empathy and Emotional Empathy in Human Behavior and Evolution. *Psychol. Rec.* **2006**, *56*, 3–21. [CrossRef]
8. Cotter, J.; Granger, K.; Backx, R.; Hobbs, M.; Looi, C.Y.; Barnett, J.H. Social cognitive dysfunction as a clinical marker: A systematic review of meta-analyses across 30 clinical conditions. *Neurosci. Biobehav. Rev.* **2018**, *84*, 92–99. [CrossRef] [PubMed]
9. Santamaría-García, H.; Baez, S.; Gómez, C.; Rodríguez-Villagra, O.; Huepe, D.; Portela, M.; Reyes, P.; Klahr, J.; Matallana, D.; Ibanez, A. The role of social cognition skills and social determinants of health in predicting symptoms of mental illness. *Transl. Psychiatry* **2020**, *10*, 165. [CrossRef]
10. Bellido-Zanin, G.; Pérez-San-Gregorio, M.Á.; Martín-Rodríguez, A.; Vázquez-Morejón, A.J. Social functioning as a predictor of the use of mental health resources in patients with severe mental disorder. *Psychiatry Res.* **2015**, *230*, 189–193. [CrossRef] [PubMed]
11. Lulla, R.; Christov-Moore, L.; Vaccaro, A.; Reggente, N.; Iacoboni, M.; Kaplan, J.T. Empathy from dissimilarity: Multivariate pattern analysis of neural activity during observation of somatosensory experience. *Imaging Neurosci.* **2024**, *2*, 1–12. [CrossRef] [PubMed]
12. Lamm, C.; Majdandžić, J. The role of shared neural activations, mirror neurons, and morality in empathy—A critical comment. *Neurosci. Res.* **2015**, *90*, 15–24. [CrossRef] [PubMed]
13. Bekkali, S.; Youssef, G.J.; Donaldson, P.H.; Albein-Urios, N.; Hyde, C.; Enticott, P.G. Is the Putative Mirror Neuron System Associated with Empathy? A Systematic Review and Meta-Analysis. *Neuropsychol. Rev.* **2021**, *31*, 14–57. [CrossRef]
14. Chartrand, T.L.; Bargh, J.A. The chameleon effect: The perception-behavior link and social interaction. *J. Personal. Soc. Psychol.* **1999**, *76*, 893–910. [CrossRef]
15. Lakin, J.L.; Chartrand, T.L. Using nonconscious behavioral mimicry to create affiliation and rapport. *Psychol. Sci.* **2003**, *14*, 334–339. [CrossRef]
16. Meltzoff, A.N.; Decety, J. What imitation tells us about social cognition: A rapprochement between developmental psychology and cognitive neuroscience. *Philos. Trans. R. Soc. B* **2003**, *358*, 491–500. [CrossRef]
17. Sperduti, M.; Guionnet, S.; Fossati, P.; Nadel, J. Mirror Neuron System and Mentalizing System connect during online social interaction. *Cogn. Processes* **2014**, *15*, 307. [CrossRef]
18. Lhermitte, F. 'Utilization Behaviour' and its Relation to Lesions of the Frontal Lobe. *Brain* **1983**, *106*, 237–255. [CrossRef]
19. Frith, C.D.; Singer, T. Review. The role of social cognition in decision making. *Philos. Trans. R. Soc. B Biol. Sci.* **2008**, *363*, 3875–3886. [CrossRef]
20. Gallese, V. Before and below "theory of mind": Embodied simulation and the neural correlates of social cognition. *Philos. Trans. R. Soc. B Biol. Sci.* **2007**, *362*, 659–669. [CrossRef] [PubMed]
21. Obhi, S.S. The amazing capacity to read intentions from movement kinematics. *Front. Hum. Neurosci.* **2012**, *6*, 162. [CrossRef] [PubMed]
22. Schulte-Rüther, M.; Markowitsch, H.J.; Fink, G.R.; Piefke, M. Mirror neuron and theory of mind mechanisms involved in face-to-face interactions: A functional magnetic resonance imaging approach to empathy. *J. Cogn. Neurosci.* **2007**, *19*, 1354–1372. [CrossRef] [PubMed]
23. Guidali, G.; Picardi, M.; Franca, M.; Caronni, A.; Bolognini, N. The social relevance and the temporal constraints of motor resonance in humans. *Sci. Rep.* **2023**, *13*, 15933. [CrossRef] [PubMed]
24. Christov-Moore, L.; Conway, P.; Iacoboni, M. Deontological Dilemma Response Tendencies and Sensorimotor Representations of Harm to Others. *Front. Integr. Neurosci.* **2017**, *11*, 34. [CrossRef]
25. Camerer, C.F. Strategizing in the Brain. *Science* **2003**, *300*, 1673–1675. [CrossRef]

26. Hewig, J.; Kretschmer, N.; Trippe, R.H.; Hecht, H.; Coles, M.G.H.; Holroyd, C.B.; Miltner, W.H.R. Why humans deviate from rational choice. *Psychophysiology* **2011**, *48*, 507–514. [CrossRef]
27. Greene, J.D. An fMRI Investigation of Emotional Engagement in Moral Judgment. *Science* **2001**, *293*, 2105–2108. [CrossRef]
28. Oullier, O.; Basso, F. Embodied economics: How bodily information shapes the social coordination dynamics of decision-making. *Philos. Trans. R. Soc. B Biol. Sci.* **2010**, *365*, 291–301. [CrossRef]
29. Van't Wout, M.; Kahn, R.S.; Sanfey, A.G.; Aleman, A. Affective state and decision-making in the Ultimatum Game. *Exp. Brain Res.* **2006**, *169*, 564–568. [CrossRef]
30. Christov-Moore, L.; Sugiyama, T.; Grigaityte, K.; Iacoboni, M. Increasing generosity by disrupting prefrontal cortex. *Soc. Neurosci.* **2017**, *12*, 174–181. [CrossRef]
31. Avenanti, A.; Minio-Paluello, I.; Bufalari, I.; Aglioti, S.M. The pain of a model in the personality of an onlooker: Influence of state-reactivity and personality traits on embodied empathy for pain. *NeuroImage* **2009**, *44*, 275–283. [CrossRef]
32. Jabbi, M.; Swart, M.; Keysers, C. Empathy for positive and negative emotions in the gustatory cortex. *NeuroImage* **2007**, *34*, 1744–1753. [CrossRef] [PubMed]
33. Pfeifer, J.H.; Iacoboni, M.; Mazziotta, J.C.; Dapretto, M. Mirroring others' emotions relates to empathy and interpersonal competence in children. *NeuroImage* **2008**, *39*, 2076–2085. [CrossRef] [PubMed]
34. Martínez-Pernía, D.; Cea, I.; Troncoso, A.; Blanco, K.; Calderón Vergara, J.; Baquedano, C.; Vergara, M. "I am feeling tension in my whole body": An experimental phenomenological study of empathy for pain. *Front. Psychol.* **2023**, *13*, 999227. [CrossRef] [PubMed]
35. Gallo, S.; Paracampo, R.; Müller-Pinzler, L.; Severo, M.C.; Blömer, L.; Fernandes-Henriques, C.; Gazzola, V. The causal role of the somatosensory cortex in prosocial behaviour. *eLife* **2018**, *7*, e32740. [CrossRef]
36. Hein, G.; Lamm, C.; Brodbeck, C.; Singer, T. Skin conductance response to the pain of others predicts later costly helping. *PLoS ONE* **2011**, *6*, e22759. [CrossRef]
37. Morelli, S.A.; Rameson, L.T.; Lieberman, M.D. The neural components of empathy: Predicting daily prosocial behavior. *Soc. Cogn. Affect. Neurosci.* **2014**, *9*, 39–47. [CrossRef]
38. Ma, Y.; Wang, C.; Han, S. Neural responses to perceived pain in others predict real-life monetary donations in different socioeconomic contexts. *NeuroImage* **2011**, *57*, 1273–1280. [CrossRef]
39. Contreras-Huerta, L.S.; Coll, M.P.; Bird, G.; Yu, H.; Prosser, A.; Lockwood, P.L.; Apps, M.A. Neural representations of vicarious rewards are linked to interoception and prosocial behaviour. *NeuroImage* **2023**, *269*, 119881. [CrossRef]
40. Cheng, Y.; Chen, C.; Lin, C.P.; Chou, K.H.; Decety, J. Love hurts: An fMRI study. *NeuroImage* **2010**, *51*, 923–929. [CrossRef]
41. Cross, K.A.; Iacoboni, M. To imitate or not: Avoiding imitation involves preparatory inhibition of motor resonance. *NeuroImage* **2014**, *91*, 228–236. [CrossRef]
42. Cuadrado, E.; Tabernero, C.; Hidalgo-Muñoz, A.R.; Luque, B.; Castillo-Mayén, R. The Arousal Effect of Exclusionary and Inclusionary Situations on Social Affiliation Motivation and Its Subsequent Influence on Prosocial Behavior. *Front. Psychol.* **2021**, *12*, 594440. [CrossRef]
43. Gu, X.; Han, S. Attention and reality constraints on the neural processes of empathy for pain. *NeuroImage* **2007**, *36*, 256–267. [CrossRef]
44. Guo, X.; Zheng, L.; Zhang, W.; Zhu, L.; Li, J.; Wang, Q.; Dienes, Z.; Yang, Z. Empathic neural responses to others' pain depend on monetary reward. *Soc. Cogn. Affect. Neurosci.* **2012**, *7*, 535–541. [CrossRef]
45. Hein, G.; Singer, T. I feel how you feel but not always: The empathic brain and its modulation. *Curr. Opin. Neurobiol.* **2008**, *18*, 153–158. [CrossRef]
46. Lamm, C.; Tomova, L. The neural bases of empathy in humans. In *Neuronal Correlates of Empathy*; Meyza, K.Z., Knapska, E., Eds.; Academic Press: Cambridge, MA, USA, 2018; pp. 25–36. [CrossRef]
47. Loggia, M.L.; Mogil, J.S.; Bushnell, C.M. Empathy hurts: Compassion for another increases both sensory and affective components of pain perception. *Pain* **2008**, *136*, 168–176. [CrossRef] [PubMed]
48. Losin, E.A.R.; Iacoboni, M.; Martin, A.; Cross, K.A.; Dapretto, M. Race modulates neural activity during imitation. *NeuroImage* **2012**, *59*, 3594–3603. [CrossRef]
49. Losin, E.A.R.; Cross, K.A.; Iacoboni, M.; Dapretto, M. Neural processing of race during imitation: Self-Similarity Versus Social Status. *Hum. Brain Mapp.* **2014**, *35*, 1723–1739. [CrossRef] [PubMed]
50. Losin, E.A.R.; Woo, C.W.; Krishnan, A.; Wager, T.D.; Iacoboni, M.; Dapretto, M. Brain and psychological mediators of imitation: Sociocultural versus physical traits. *Cult. Brain* **2015**, *3*, 93–111. [CrossRef]
51. Singer, T.; Seymour, B.; O'Doherty, J.P.; Stephan, K.E.; Dolan, R.J.; Frith, C.D. Empathic neural responses are modulated by the perceived fairness of others. *Nature* **2006**, *439*, 466–469. [CrossRef] [PubMed]
52. Stevens, F.; Taber, K. The neuroscience of empathy and compassion in pro-social behavior. *Neuropsychologia* **2021**, *159*, 107925. [CrossRef] [PubMed]

53. Bukowski, H.; Todorova, B.; Boch, M.; Silani, G.; Lamm, C. Socio-cognitive training impacts emotional and perceptual self-salience but not self-other distinction. *Acta Psychol.* **2021**, *216*, 103297. [CrossRef] [PubMed]
54. Raz, G.; Jacob, Y.; Gonen, T.; Winetraub, Y.; Flash, T.; Soreq, E.; Hendler, T. Cry for her or cry with her: Context-dependent dissociation of two modes of cinematic empathy reflected in network cohesion dynamics. *Soc. Cogn. Affect. Neurosci.* **2014**, *9*, 30–38. [CrossRef] [PubMed]
55. Zaki, J.; Weber, J.; Bolger, N.; Ochsner, K. The neural bases of empathic accuracy. *Proc. Natl. Acad. Sci. USA* **2009**, *106*, 11382–11387. [CrossRef]
56. Spunt, R.P.; Lieberman, M.D. The Busy Social Brain: Evidence for Automaticity and Control in the Neural Systems Supporting Social Cognition and Action Understanding. *Psychol. Sci.* **2013**, *24*, 80–86. [CrossRef]
57. Wu, X.; Kong, Y.Z.; Hu, L. Neural network dynamics underlying the bottom-up perception and top-down regulation processes of empathy. *Imaging Neurosci.* **2025**, *3*, IMAG.a.972. [CrossRef]
58. Ebisch, S.J.H.; Scalabrini, A.; Northoff, G.; Mucci, C.; Sergi, M.R.; Saggino, A.; Aquino, A.; Alparone, F.R.; Perrucci, M.G.; Gallese, V.; et al. Intrinsic Shapes of Empathy: Functional Brain Network Topology Encodes Intersubjective Experience and Awareness Traits. *Brain Sci.* **2022**, *12*, 477. [CrossRef]
59. Lamm, C.; Decety, J.; Singer, T. Meta-analytic evidence for common and distinct neural networks associated with directly experienced pain and empathy for pain. *NeuroImage* **2011**, *54*, 2492–2502. [CrossRef]
60. Shamay-Tsoory, S.G.; Aharon-Peretz, J.; Perry, D. Two systems for empathy: A double dissociation between emotional and cognitive empathy in inferior frontal gyrus versus ventromedial prefrontal lesions. *Brain* **2009**, *132*, 617–627. [CrossRef]
61. Feng, C.; Yuan, J.; Geng, H.; Gu, R.; Zhou, H.; Wu, X.; Luo, Y. Individualized prediction of trait narcissism from whole-brain resting-state functional connectivity. *Hum. Brain Mapp.* **2018**, *39*, 3701–3712. [CrossRef]
62. Bellucci, G.; Hahn, T.; Deshpande, G.; Krueger, F. Functional connectivity of specific resting-state networks predicts trust and reciprocity in the trust game. *Cogn. Affect. Behav. Neurosci.* **2019**, *19*, 165–176. [CrossRef]
63. Roccas, S.; Sagiv, L.; Schwartz, S.H.; Knafo, A. The Big Five Personality Factors and Personal Values. *Personal. Soc. Psychol. Bull.* **2002**, *28*, 789–801. [CrossRef]
64. Nostro, A.D.; Müller, V.I.; Varikuti, D.P.; Pläschke, R.N.; Hoffstaedter, F.; Langner, R.; Patil, K.R.; Eickhoff, S.B. Predicting personality from network-based resting-state functional connectivity. *Brain Struct. Funct.* **2018**, *223*, 2699–2719. [CrossRef] [PubMed]
65. Spies, M.; Hahn, A.; Kranz, G.S.; Sladky, R.; Kaufmann, U.; Hummer, A.; Ganger, S.; Kraus, C.; Winkler, D.; Seiger, R.; et al. Gender transition affects neural correlates of empathy: A resting state functional connectivity study with ultra high-field 7T MR imaging. *NeuroImage* **2016**, *138*, 257–265. [CrossRef] [PubMed]
66. Abram, S.V.; Wisner, K.M.; Fox, J.M.; Barch, D.M.; Wang, L.; Csernansky, J.G.; MacDonald, A.W.; Smith, M.J. Fronto-temporal connectivity predicts cognitive empathy deficits and experiential negative symptoms in schizophrenia. *Hum. Brain Mapp.* **2017**, *38*, 1111–1124. [CrossRef] [PubMed]
67. Esménio, S.; Soares, J.M.; Zeidman, P.; Razi, A.; Gonçalves, Ó.F.; Friston, K.; Coutinho, J. Using resting-state DMN effective connectivity to characterize the neurofunctional architecture of empathy. *Sci. Rep.* **2019**, *9*, 2603. [CrossRef]
68. Stoica, T.; Depue, B. Shared Characteristics of Intrinsic Connectivity Networks Underlying Interoceptive Awareness and Empathy. *Front. Hum. Neurosci.* **2020**, *14*, 571070. [CrossRef]
69. Mehling, W.E.; Acree, M.; Stewart, A.; Silas, J.; Jones, A. The Multidimensional Assessment of Interoceptive Awareness, Version 2 (MAIA-2). *PLoS ONE* **2018**, *13*, e0208034. [CrossRef] [PubMed] [PubMed Central]
70. Winters, D.E.; Pruitt, P.J.; Fukui, S.; Cyders, M.A.; Pierce, B.J.; Lay, K.; Damoiseaux, J.S. Network functional connectivity underlying dissociable cognitive and affective components of empathy in adolescence. *Neuropsychologia* **2021**, *156*, 107832. [CrossRef]
71. Winters, D.E.; Pruitt, P.; Damoiseaux, J.; Sakai, J.T. Callous-unemotional traits in adolescents moderate neural network associations with empathy. *Psychiatry Res. Neuroimaging* **2022**, *320*, 111429. [CrossRef]
72. Winters, D.E.; Guha, A.; Sakai, J.T. Connectome-based predictive modeling of empathy in adolescents with and without the low-prosocial emotion specifier. *Neurosci. Lett.* **2023**, *812*, 137371. [CrossRef]
73. Bray, K.O.; Pozzi, E.; Vijayakumar, N.; Richmond, S.; Seal, M.; Pantelis, C.; Anderson, V.; Whittle, S. Empathy and resting-state functional connectivity in children. *Neuroimage Rep.* **2022**, *2*, 100142. [CrossRef]
74. McLaren, D.G.; Ries, M.L.; Xu, G.; Johnson, S.C. A generalized form of context-dependent psychophysiological interactions (gPPI): A comparison to standard approaches. *NeuroImage* **2012**, *61*, 1277–1286. [CrossRef]
75. Reggente, N.; Moody, T.D.; Morfini, F.; Sheen, C.; Rissman, J.; O'Neill, J.; Feusner, J.D. Multivariate resting-state functional connectivity predicts response to cognitive behavioral therapy in obsessive–compulsive disorder. *Proc. Natl. Acad. Sci. USA* **2018**, *115*, 2222–2227. [CrossRef]
76. Christov-Moore, L.; Reggente, N.; Douglas, P.K.; Feusner, J.D.; Iacoboni, M. Predicting Empathy From Resting State Brain Connectivity: A Multivariate Approach. *Front. Integr. Neurosci.* **2020**, *14*, 3. [CrossRef]

77. Hilbert, K.; Böhnlein, J.; Meinke, C.; Chavanne, A.V.; Langhammer, T.; Stumpe, L.; Winter, N.; Leenings, R.; Adolph, D.; Arolt, V.; et al. Lack of evidence for predictive utility from resting state fMRI data for individual exposure-based cognitive behavioral therapy outcomes: A machine learning study in two large multi-site samples in anxiety disorders. *NeuroImage* **2024**, *295*, 120639. [CrossRef]
78. Finn, E.S. Is it time to put rest to rest? *Trends Cogn. Sci.* **2021**, *25*, 1021–1032. [CrossRef] [PubMed Central]
79. Litvack-Miller, W.; McDougall, D.; Romney, D.M. The structure of empathy during middle childhood and its relationship to prosocial behavior. *Genet. Soc. Gen. Psychiatry* **1997**, *123*, 303–324.
80. Kelly, R.E.J.; Alexopoulos, G.S.; Wang, Z.; Gunning, F.M.; Murphy, C.F.; Morimoto, S.S.; Hoptman, M.J. Visual inspection of independent components: Defining a procedure for artifact removal from fMRI data. *J. Neurosci. Methods* **2010**, *189*, 233–245. [CrossRef]
81. Power, J.D.; Cohen, A.L.; Nelson, S.M.; Wig, G.S.; Barnes, K.A.; Church, J.A.; Petersen, S.E. Functional Network Organization of the Human Brain. *Neuron* **2011**, *72*, 665–678. [CrossRef]
82. Iacoboni, M. Neural mechanisms of imitation. *Curr. Opin. Neurobiol.* **2005**, *15*, 632–637. [CrossRef] [PubMed]
83. Banks, S.J.; Eddy, K.T.; Angstadt, M.; Nathan, P.J.; Luan Phan, K. Amygdala-frontal connectivity during emotion regulation. *Soc. Cogn. Affect. Neurosci.* **2007**, *2*, 303–312. [CrossRef]
84. Brighina, F.; Tommaso, M.D.; Giglia, F.; Scalia, S.; Cosentino, G.; Puma, A.; Panetta, M.; Giglia, G.; Fierro, B. Modulation of pain perception by transcranial magnetic stimulation of left prefrontal cortex. *J. Headache Pain* **2011**, *12*, 185–191. [CrossRef]
85. Cho, S.S.; Strafella, A.P. rTMS of the left dorsolateral prefrontal cortex modulates dopamine release in the ipsilateral anterior cingulate cortex and orbitofrontal cortex. *PLoS ONE* **2009**, *4*, e6725. [CrossRef]
86. Decety, J.; Lamm, C. The role of the right temporoparietal junction in social interaction: How low-level computational processes contribute to meta-cognition. *Neuroscientist* **2007**, *13*, 580–593. [CrossRef]
87. Miller, E.K.; Cohen, J.D. An Integrative Theory of Prefrontal Cortex Function. *Annu. Rev. Neurosci.* **2001**, *24*, 167–202. [CrossRef]
88. Spengler, S.; von Cramon, D.Y.; Brass, M. Resisting motor mimicry: Control of imitation involves processes central to social cognition in patients with frontal and temporo-parietal lesions. *Soc. Neurosci.* **2010**, *5*, 401–416. [CrossRef]
89. Tassy, S.; Oullier, O.; Duclos, Y.; Coulon, O.; Mancini, J.; Deruelle, C.; Wicker, B. Disrupting the right prefrontal cortex alters moral judgement. *Soc. Cogn. Affect. Neurosci.* **2012**, *7*, 282–288. [CrossRef]
90. Volman, I.; Roelofs, K.; Koch, S.; Verhagen, L.; Toni, I. Anterior prefrontal cortex inhibition impairs control over social emotional actions. *Curr. Biol.* **2011**, *21*, 1766–1770. [CrossRef]
91. Winecoff, A.; Clithero, J.A.; Carter, R.M.; Bergman, S.R.; Wang, L.; Huettel, S.A. Ventromedial prefrontal cortex encodes emotional value. *J. Neurosci.* **2013**, *33*, 11032–11039. [CrossRef]
92. Benjamini, Y.; Hochberg, Y. Controlling the false discovery rate: A practical and powerful approach to multiple testing. *J. R. Stat. Soc. Ser. B* **1995**, *57*, 289–300. [CrossRef]
93. Caes, L.; Goubert, L.; Devos, P.; Verlooy, J.; Benoit, Y.; Vervoort, T. Personal Distress and Sympathy Differentially Influence Health Care Professional and Parents' Estimation of Child Procedure-Related Pain. *Pain Med.* **2017**, *18*, 275–282. [CrossRef] [PubMed]
94. Eisenberg, N.; Fabes, R.A.; Miller, P.A.; Fultz, J.; Shell, R.; Mathy, R.M.; Reno, R.R. Relation of sympathy and personal distress to prosocial behavior: A multimethod study. *J. Personal. Soc. Psychol.* **1989**, *57*, 55–66. [CrossRef]
95. Decety, J.; Lamm, C. Empathy versus Personal Distress: Recent Evidence from Social Neuroscience. In *The Social Neuroscience of Empathy*; Decety, J., Ickes, W., Eds.; MIT Press: Cambridge, MA, USA, 2009.
96. Christov-Moore, L.; Simpson, E.A.; Coudé, G.; Grigaityte, K.; Iacoboni, M.; Ferrari, P.F. Empathy: Gender effects in brain and behavior. *Neurosci. Biobehav. Rev.* **2014**, *46*, 604–627. [CrossRef]
97. Botvinik-Nezer, R.; Holzmeister, F.; Camerer, C.F.; Dreber, A.; Huber, J.; Johannesson, M.; Kirchler, M.; Iwanir, R.; Mumford, J.A.; Adcock, R.A.; et al. Variability in the analysis of a single neuroimaging dataset by many teams. *Nature* **2020**, *582*, 84–88. [CrossRef]
98. Bowring, A.; Nichols, T.E.; Maumet, C. Isolating the sources of pipeline-variability in group-level task-fMRI results. *Hum. Brain Mapp.* **2022**, *43*, 1112–1128. [CrossRef]
99. Baker, M. Is there a reproducibility crisis? A Nature survey lifts the lid on how researchers view the 'crisis' rocking science and what they think will help. *Nat. News* **2016**, *533*, 452–454. [CrossRef]
100. Schmidt, S. Shall we Really do it Again? The Powerful Concept of Replication is Neglected in the Social Sciences. *Rev. Gen. Psychol.* **2009**, *13*, 90–100. [CrossRef]
101. Zwaan, R.A.; Etz, A.; Lucas, R.E.; Donnellan, M.B. Making replication mainstream. *Behav. Brain Sci.* **2018**, *41*, e120. [CrossRef]